Published by IOP Publishing for Sissa Medialab

Received: *March 31, 2017*
Accepted: *May 18, 2017*
Published: *May 31, 2017*

2017 JINST 12 P05024

The hard X-ray Photon Single-Shot Spectrometer of SwissFEL — initial characterization

J. Rehanek,[1] M. Makita,[2] P. Wiegand, P. Heimgartner, C. Pradervand, G. Seniutinas, U. Flechsig, V. Thominet, C.W. Schneider, A. Rodriguez Fernandez, C. David, L. Patthey and P. Juranić

Paul-Scherrer Institute,
5232 Villigen-PSI, Switzerland

E-mail: Jens.Rehanek@psi.ch

Abstract: SwissFEL requires the monitoring of the photon spectral distribution at a repetition rate of 100 Hz for machine optimization and experiment online diagnostics. The Photon Single Shot Spectrometer has been designed for the photon energy range of 4 keV to 12 keV provided by the Aramis beamline. It is capable of measuring the spectrum in a non-destructive manner, with an energy resolution of $\Delta E/E = (2\text{–}5) \times 10^{-5}$ over a bandwidth of 0.5% on a shot-to-shot basis. This article gives a detailed description about the technical challenges, structures, and considerations when building such a device, and to further enhance the performance of the spectrometer.

Keywords: Beam-line instrumentation (beam position and profile monitors; beam-intensity monitors; bunch length monitors); Instrumentation for FEL

[1]Corresponding author.
[2]Present address: European XFEL GmbH, Holzkoppel 4, 22869 Schenefeld, Germany.

doi:10.1088/1748-0221/12/05/P05024

Contents

2017 JINST 12 P05024

1 Introduction

SwissFEL, like all self-amplified spontaneous emission Free Electron Lasers (SASE FEL), will generate X-ray radiation that varies from shot to shot both in spectrum and intensity [1, 2]. These variations require a characterization of each pulse with high precision in order to deliver reliable information to the users, enabling them to improve their data quality by normalization with the incoming spectrum on a shot-to-shot basis. Moreover, such a device can provide valuable feedback to the operators for tuning the machine parameters. Since the width of the spectral spikes in a SASE spectrum is linked to the length of the X-ray pulses, high resolution spectral measurements can also serve to determine the pulse duration.

For the photon energy range of hard X-rays at XFELs there have been several techniques proposed and applied for single-shot measurements. At SACLA in Japan, a non-online concept was developed using a focusing plane-elliptical mirror to create a diverging beam, spectrally measured using an analyzer crystal [3–5]. At LCLS in the United States of America, a single bent crystal spectrometer was investigated [6, 7] and applied [8]. A similar principle is used for the MID experiment of the European XFEL [9]. PSI has developed a focusing transmission grating spectrometer in close collaboration with LCLS [10]. As an online device operated at SACLA, a combination of a transmission grating [10] and the previous concept [3] is integrated in [11]. Another approach of employing Reflective Zone Plates was proposed by HZB in Germany [12, 13], and its potential applications are further investigated [14–16].

The Hard X-ray Photon Single-Shot Spectrometer of PSI (PSSS) uses the concept of combining the diffraction grating [17] and a high resolution analyzer crystal foil [6], as described and tested in [18], to deliver high-resolution spectral information between 4 and 12 keV for every pulse. PSSS also includes an option for intensity correction of the generated spectrum, which is of high interest to modern experimental techniques such as RIXS, REXS, XAS, XES, and others [19].

This paper describes the overall design and the key components of the PSSS, and how to test and install them. These key components are, in order of appearance in this manuscript, diamond gratings, calibration foils, the profile monitor (Ce:YAG-screen), and the bent Si crystals. The set of diamond gratings is installed and generate the 0^{th} and the $\pm 1^{st}$ diffraction orders in the horizontal plane. The transmitted (0^{th} order) beam carries negligible disturbance by the gratings to the experiment. The spectral distribution will not be affected by insertion of the gratings. They will be more than 95% transmissive to the 0^{th} order and they are homogeneous, thus also the intensity distribution within the beam is not affected. The $+1^{st}$ order hits a thin silicon crystal, where it is Bragg-reflected and spectrally dispersed, upwards, orthogonal to the dispersive direction of the gratings. The light subsequently passes through a Beryllium window and a He-filled tube to a Ce:YAG scintillator screen and read out with a fast frame imaging camera. For fast read-out, the PSSS uses a PCO.edge 5.5 camera with 6.5 μm size pixels, in combination with an optical magnification factor of about 3. Simultaneously, the -1^{st} order beam is designed to directly hit another Ce:YAG scintillator screen coupled to a Basler acA800-200gm camera, in order to record the intensity distribution of the photon pulses. This information will be used to perform a normalization of the resulting spectra.

2 Instrument design

In this section we present and discuss the crucial components, physical principles and considerations building the photon single-shot spectrometer for SwissFEL. Figure 1 shows the basic idea of the PSSS. The component distances for setting the PSSS are: 650 mm grating to profile monitor (Ce:YAG), 4 m grating to crystal, and 1 m crystal to detector-system.

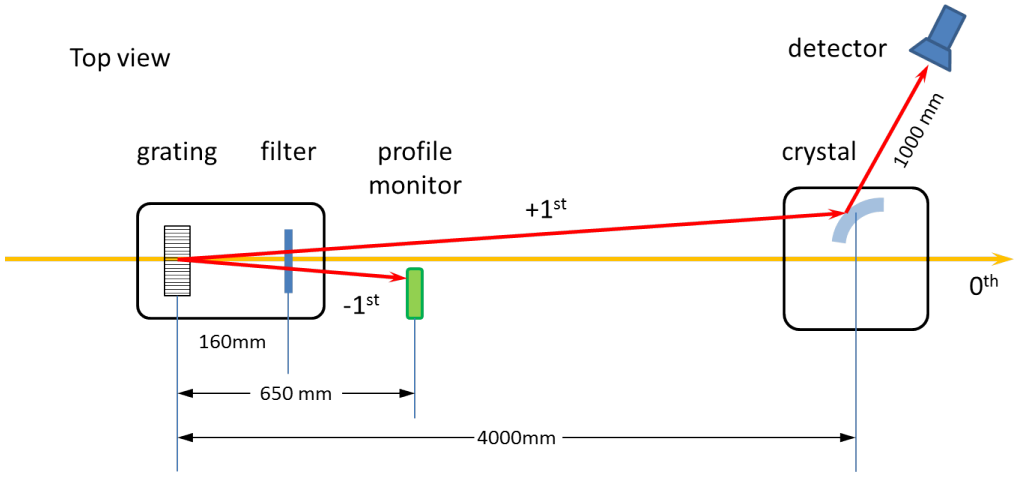

Figure 1. Schematic design of PSSS. The $+1^{st}$ order of diffraction is Bragg-reflected upwards to the detector.

2.1 Diamond transmission gratings

The first component of PSSS that sees the light from SwissFEL is a diamond transmission grating, the fabrication process of which is described in [17]. This grating splits a small portion of X-rays as the 1st order diffracted beam that goes to the spectrometer, leaving the transmitted beam undisturbed for experiments downstream. This beam splitting allows for non-destructive, online measurements. We employ a set of gratings of three different pitches that cover the acceptable diffraction angles over the entire X-ray energy range: 100 nm and 150 nm pitches with structure depths of 0.7–0.8 μm, and 200 nm pitches with the depth of 1 μm. For the range of 4–8 keV the 200 nm or 150 nm pitch gratings are used. The PSSS uses the 150 nm grating for the 8–10 keV range, while the 100 nm pitch is used for energies above 10 keV. In our instrument, the gratings are located next to each other, exchangeable by a moveable linear stage, moving in and out the grating according to the photon energy range of interest. This movement is done independently of the bent crystal and detector.

The effective height of the grating structure, and with it the diffraction efficiency, is tunable by tilting the gratings relative to the incoming FEL beam, as presented in [20]. The gratings are tilted around the axis perpendicular to the direction of the grating lines. Hence this does not result in change of divergence angle of the diffraction orders. The ability to tilt the gratings up to 60°allows for the doubling of the effective height of the structure, thus quadrupling the grating efficiency at the cost of increasing the effective thickness of the diamond grating membrane, hence slightly lowering the 0th order transmission. The separation between the 0th and the 1st order diffraction at the position of the bent Si crystal varies depending on the pitch of the gratings and the incoming photon energy, described by the grating equation at normal incidence:

$$n\lambda = g \sin \varphi_n \tag{2.1}$$

with n being the diffraction order, λ the wavelength, g the grating pitch, and φ_n the angle of deviation of the maximum. The corresponding geometric relation is then given by:

$$d = a \tan \varphi_n \tag{2.2}$$

with d being the distance between 0th and 1st order, and a the distance between grating and crystal. In case of the PSSS at SwissFEL, a is 4 m.

2.2 Thin silicon crystals

Once the beam has passed the grating, the +1st order diffraction hits a bent silicon crystal and is Bragg-reflected, resulting in energy-resolved high resolution spectra. The factors that affect the energy resolution of the crystal spectrometer are the bent crystal's thickness, the applied bending radius, and the choice of the crystal plane for Bragg-reflection.

2.2.1 Crystal thickness

The relation between the thickness of the crystal and the resulting width of the Bragg reflection follows:

$$w = t \cos \theta_B \tag{2.3}$$

where w denotes the width, t the crystal thickness, and θ_B the Bragg angle for a given photon energy, as shown in figure 2. The smearing of the spectra is, up to certain limit, proportional to the thickness

2017 JINST 12 P05024

of the crystal. This is due to the contribution from the deeper layers. Also other effects like crystal strain and anticlastic distortions start playing a role when using thicker crystals. Here, based on previous reports [21], the PSSS uses a 10 μm thick crystal, to get the best energy resolution possible.

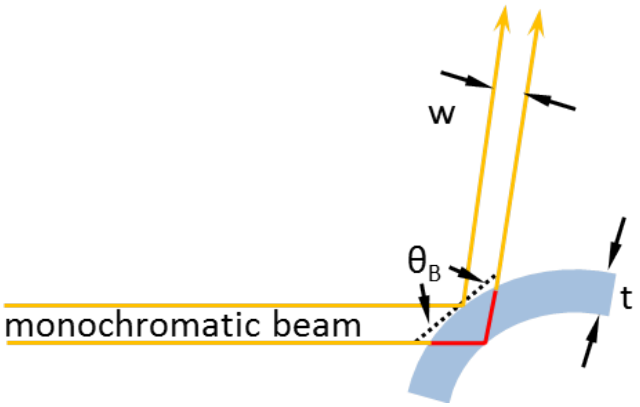

Figure 2. Contribution of the crystal's thickness to the width of the Bragg-reflected beam.

2.2.2 Bending radius, Bragg-reflection

When an X-ray beam with a known divergence and a small bandwidth irradiates the convex side of a bent crystal, each wavelength that satisfies the Bragg condition is reflected and spectrally dispersed radially away from the center of the bending circle, as shown in figure 3. Each part of the beam would satisfy the Bragg condition for a slightly different wavelength, according to the equation $n\lambda_\iota = 2d \sin\theta_{B,i}$, where d is the lattice spacing, $\theta_{B,i}$ the Bragg angle, and i denotes each of the different wavelengths inside the photon beam. The divergence of SwissFEL is expected to be in the order of 1 μrad to 6.4 μrad over the entire range of photon energies, thus negligible. The spectral dispersion of the Bragg diffracted pulse on the detector plane Δx for an energy interval ΔE is given by:

$$\Delta x = 2\tan\theta_{B,i}\left(\frac{r\,\sin\theta_{B,i}}{2} + L\right)\frac{\Delta E}{E} \tag{2.4}$$

with L being the distance from the crystal to the detector. The maximum ΔE for a given bent crystal depends on the size of the incoming X-ray beam s and the radius of curvature r (as shown in figure 3):

$$\Delta E_{\max} = E\frac{s}{r}\frac{\cos\theta_{B,i}}{\sin^2\theta_{B,i}} \tag{2.5}$$

We make use of crystal foils with different bending radii to cover the entire range of photon energies with an energy resolution of the order of $\Delta E/E = (2\text{–}5)\times 10^{-5}$ for the beam sizes expected by the SwissFEL, and a photon energy bandwidth of 0.5%. The used reflections and corresponding bending radii are summarized in figure 4.

We are planning to use the radius 155 mm with the Si(111)-reflection for the energy range of 4 keV to 5.5 keV, and radii 75 mm, 145 mm, 200 mm with the Si(220) reflection for the range 5.5 keV up to 12 keV. In order to have a higher energy-resolution for specific applications, we will

2017 JINST 12 P05024

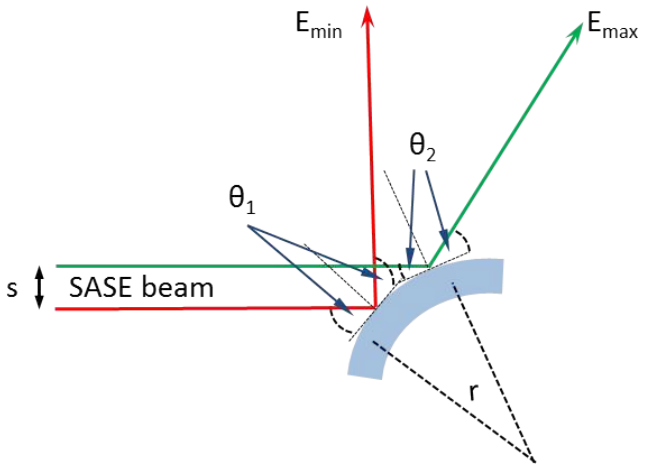

Figure 3. Relation between the maximum detectable energy range and the parameters *s* (size of the non-monochromatic beam) and *r* (radius of curvature of the crystal).

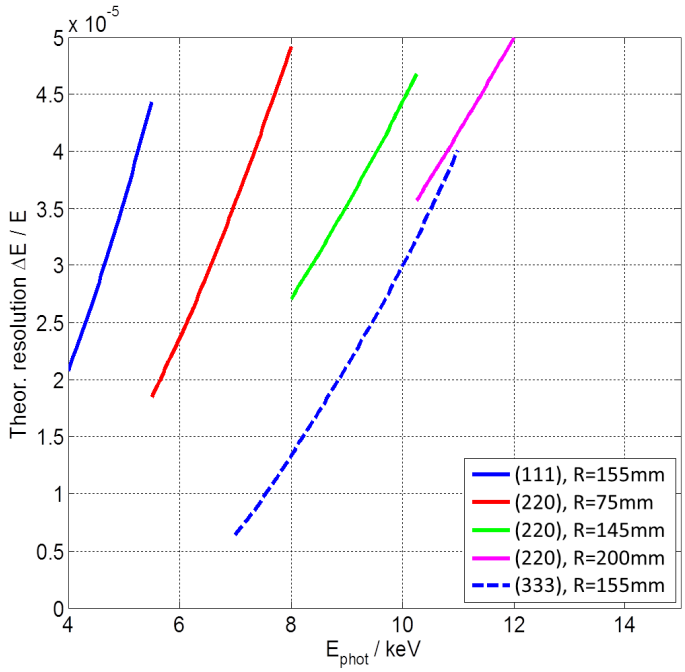

Figure 4. Theoretical resolution vs. the photon energy for the three crystal orientations. The crystal in (333) reflection does not cover 0.5% of bandwidth, but only 0.2%.

make use of the Si(111) crystal in (333)-reflection, with the small drawback of having a smaller bandwidth covered with this reflection for single-shot measurements. The bending parameters and reflections are optimized for the PCO.edge camera pixels of 6.5 μm, full detector chip dimension of 16.6 mm $\times$ 14 mm and a detector distance of 1 m from the Bragg-reflecting crystal.

2.3 Intensity profile monitor

As pointed out in the previous sections, each part of the beam in vertical direction corresponds to a certain incidence angle on the crystal and therefore to a certain photon energy. FEL sources have position and intensity jitter for each shot due to the machine instabilities. Therefore, the bent crystal spectrometer will only provide the true spectrum as long as the incoming beam is of homogeneous intensity. As shown in figure 5, any inhomogeneity in intensity will affect the measurement, as the measured intensity of a specific energy will be proportional to the intensity of the corresponding part of the beam. Moreover, any inhomogeneity in the diffraction efficiency of the diffraction grating will also affect the intensity profile of the beam hitting the bent crystal. It is therefore essential to measure the intensity profile on a shot to shot basis and to use this information to correct (normalize) the data. We use the -1^{st} order (see figure 1) of the diffraction grating, which is sent onto an intensity profile monitor.

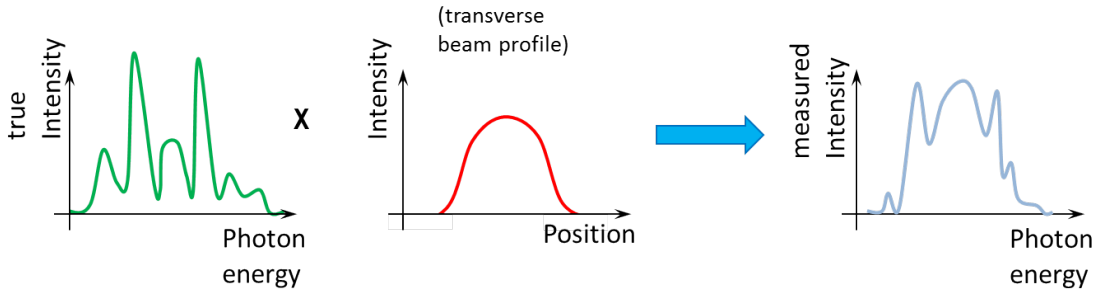

Figure 5. Intensity distribution (transverse) within the FEL-beam, which influences the intensity distribution within the measured photon energy spectrum.

The -1^{st} and 0^{th} order beams can be projected on a 25 μm Ce:YAG screen, placed between the grating and the spectrometer unit to observe the transverse intensity profiles of the beams. The difference in distance from the diffractive grating between the profile monitor and the bent crystal and the respective detector distance will be compensated by linear scaling of the size and features of the transverse beam profile. It is planned to include 3 possible different modes of inspecting with the intensity monitor: a) inspecting all 3 profiles at the same time, b) $+1^{st}$ and -1^{st} orders at the same time, c) exclusively -1^{st} order. This will be possible by inserting differently shaped screens. The screen will be inspected by an optical system and read out using a Basler camera. This information will be used to correct the intensity distribution within the photon energy spectrum.

2.4 Transmission filters

To ensure an energy calibration, the single-shot spectrometer setup is equipped with 5 thin foils for energy calibration situated between the grating and the bent crystal. To have several calibration points over the photon energy range of the SwissFEL Aramis beamline, we include materials with different calibration K-edges, such as Titanium (edge at 4.9 keV, 10 μm thick), Manganese (6.5 keV, 20 μm), Iron (7.1 keV, 10 μm), Nickel (8.3 keV, 12.5 μm), and Copper (8.9 keV, 20 μm). Insertion of these foils into the XFEL beam with a photon energy covering the absorption edge will cause a step in the measured spectra, allowing for a precise energy calibration.

2017 JINST 12 P05024

3 Experimental results and discussion

This section describes the tests of the key components for initial installation and commissioning of the PSSS. Additionally, the performance of hardware, such as motors, stages (translation and rotation), and mechanical components is described briefly.

3.1 Transmission gratings

The gratings of the PSSS have been tested at the optics beamline at SLS [24]. They show ratios ($I_{1^{st}}/I_{0^{th}}$) of 0.53% at 10 keV (pitch 200 nm), 0.7% at 8 kev (pitch 150 nm), and 2.7% at 10 keV (pitch 100 nm) in normal incidence. The measured efficiency was the same across the grating area, thus confirms the structure homogeneity of the gratings. Tilting the grating by 60° led to an increase of the ratio up to a factor of 4, as expected and predicted in [20], see figure 7.

The diffraction gratings require supporting structures to prevent collapse during the nano-lithography process, as described in [17]. The support structure is a periodic set of bars, with 10 time larger pitches compared to that of the main grating, and oriented perpendicular to the grating lines. It will also cause diffraction. However, the larger pitch will result in much smaller diffraction angles. This leads to a generation of diffracted pulses from these structures, which are typically less than a factor of 10^{-2} intensity of those originating from the main diffraction grating. Calculations also confirm, according to the normalized intensity function [23], that the intensity of the diffraction patterns from the supporting structure is several orders of magnitude smaller than those caused by the high-pitch grating.

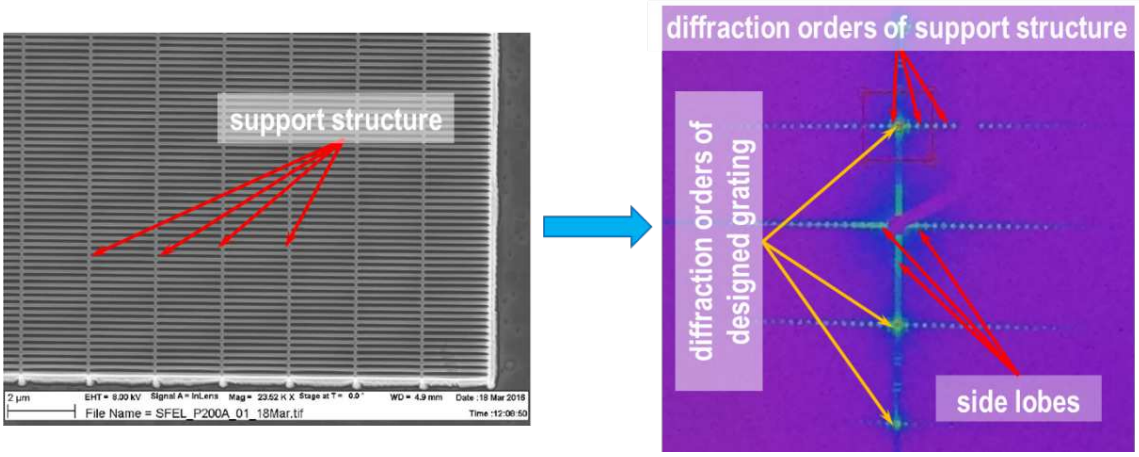

Figure 6. Left: SEM image of a grating structure (200 nm pitch), containing the supporting structure. Right: image at the detector. Note, the intensity scale is logarithmic; the dynamic range of the detection system consists of 11 orders of magnitude of intensity difference.

The unwanted stray orders, generated by both the grating and the supporting structures, will be blocked completely inside SwissFEL using a slit system 36 m further downstream.

3.2 Si-crystals

The center-piece of the PSSS is the bent Si crystals. The crystals' shape homogeneity strongly determines the obtainable spectra resolution and quality. Since these aspects are entirely dependent

2017 JINST 12 P05024

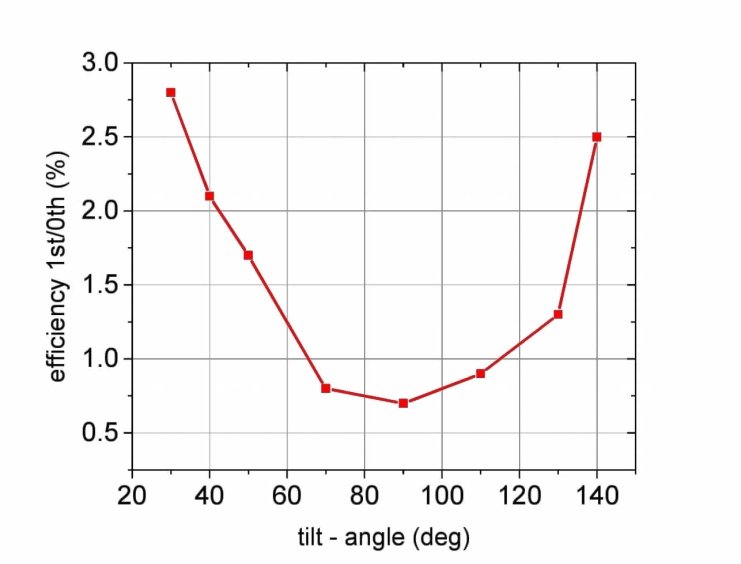

Figure 7. Effect of tilting the diamond gratings shows clearly the increase of efficiency. This measurement was performed at 8keV, using the 150 nm pitch grating.

on the bent crystal holder, special care needs to be taken in its design and manufacturing. The surface radii and waviness were tested and optimized in iterations of measurements using a white-light interferometer and re-working the surfaces in feedback with the workshop. The Si crystals are manufactured by Norcada Inc.

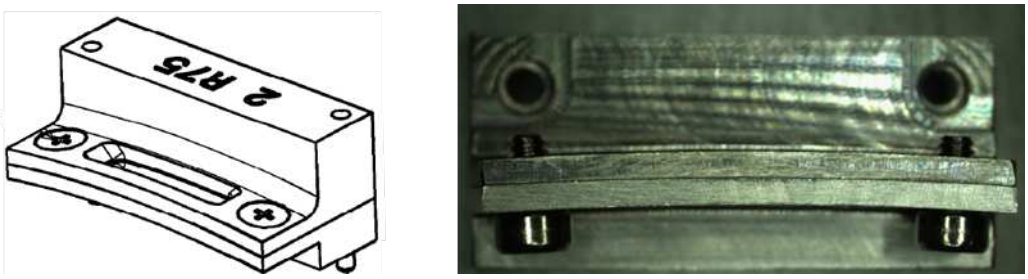

Figure 8. The design of the crystal bender. The most recent generation has very little roughness and bends the crystal exactly into the designed radius of curvature.

The effect of a non-perfect holder surface considerably affects the quality of the Bragg-reflected line observed on the detector. Figure 9 shows how a non-cylindrical bending leads to effects that complicate the evaluation of the measured spectrum, confirming the previous measurements [21]. The measurements of the surface shape and roughness of the crystal holders as well as of the bent Si-crystals were performed at a white light interferometer (WLI) "New View" from ZYGO, using a 1:1 Michelson objective. The bent silicon crystals' reflections were characterized at the Optics Beamline of the SLS [24].

During the process of manufacturing the thin Silicon crystals a miscut between the diffraction planes and the selected out-of-plane orientation of the Si crystal was generated. This miscut can lead to displacements of the Bragg-reflected beam at the detector, which can complicate the record

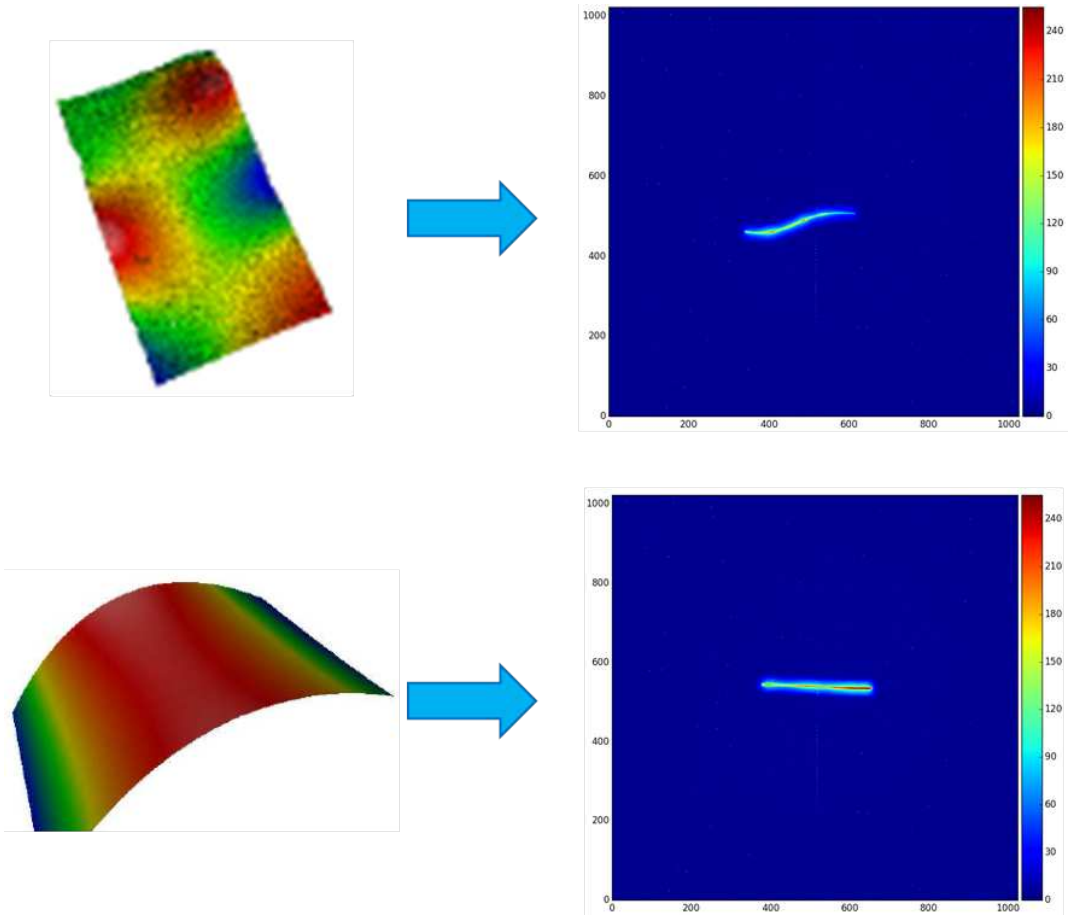

Figure 9. WLI-image of the surface (left) and Bragg-reflection on a screen (right) of the bent Si crystal (bending radius: 150 mm). Top: non-cylindrical and non-uniform shape lead to complicated shape of reflection. Bottom: perfect cylindrical shape leads to a straight line.

of the photon spectrum in the accessible range of the detector. This possible problem needs to be taken into consideration when adjusting the detector system, and should be accounted for in the controls software for the smooth operation of the PSSS.

For the spectral analysis of the FEL-beam, (110) and (111) oriented Si crystals, each 10 μm thick, are used. To determine the miscut for the two in-plane directions, ω-scans [25] were conducted using a Siemens/Bruker D500 powder diffractometer with a Cu-source equipped with long Soller slits on the detector side. This geometry enables to tune the X-ray beam consisting primarily of Cu $K_{\alpha 1}$ radiation. The (111) oriented Si 10 μm foils, with dimensions of 12.5 mm $\times$ 5 mm, were mounted with either the (100) or (1-11) in-plane orientation parallel to the X-ray beam propagation axis. The ω-scans were performed at $2\theta = 28.443°$ for the (111) Si Bragg reflection. An example for one set of ω-scans on (111) Si is shown in figure 10 where the off-set was measured to be $-0.3815°$ and $0.5785°$ for the long and short edges, respectively. The same procedure was done for (110) oriented Si foils. Each Si foil has been characterized individually prior to its mounting into the bent sample holder. The measured miscuts of all four implemented Si crystals are summarized in table 1.

A correction for the miscut is taken into consideration for running the PSSS.

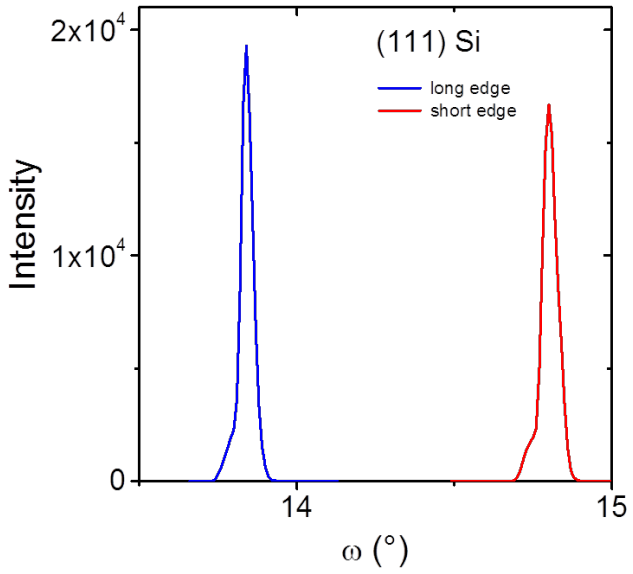

Figure 10. ω-scans to determine the miscut for the two in-plane directions of a 10 μm thick (111) oriented Si foil.

Table 1. The used Si-crystal reflections and their measured miscuts.

Si-reflection	bending radius	miscut in dispersive direction	in non-dispersive direction
111	155 mm	+0.38°	−0.58°
110	75 mm	+1.0°	+1.02°
110	145 mm	+0.9°	+0.935°
110	200 mm	+0.88°	+0.95°

3.3 Motions

The control over the precise rotational movement of the bent Si crystal is one of the most crucial parts of the PSSS for setting the Bragg angle. The rotational movement around the turning point at the crystal's surface is built and tested to rotate with a precision of better than 200 μrad rms. Also the detector arm to collect the Bragg-reflection rotates with a precision of better than 20 μrad rms. As the detector arm has to precisely follow the rotation of the bent crystals, the axes of rotation for both crystal holder and detector arm must be coaxial as well, which is measured to be within less than 10 μm rms. The gratings can be tilted by a precision of better than 1 mrad.

4 Summary

We have shown the basic principles of the Photon Single-Shot Spectrometer of SwissFEL. The most critical points in developing a reliable instrument have been described in detail and it is shown that the PSSS could fulfil the demands of the users as well as serve the machine as trustworthy feedback-instrument. All research, developments, and the test experiments have been carried out at PSI. PSSS is expected to be in full operation when first users are performing their experiments at SwissFEL.

2017 JINST 12 P05024

Acknowledgments

The authors would like to thank P. Karvinen from Finnlitho Ltd. for performing and evaluating the simulation on the properties of the crystals of PSSS for PSI, R. Ischebeck and H. Brands for support setting up the PCO.edge system, M. Lebugle for his support in experimental tests, A. Jaggi for supporting experimental preparations, N. Kujala for discussions and experimental support, and the company Heinz Baumgartner AG for manufacturing and assembly. Parts of these experiments were performed at the X05DA beamline at the Swiss Light Source, Paul Scherrer Institut, Villigen, Switzerland. This project has received funding from the EU-H2020 Research and Innovation programme under grant agreement No 654360 NFFA-Europe.

References

[1] P. Emma, K. Bane, M. Cornacchia, Z. Huang, H. Schlarb, G. Stupakov et al., *Femtosecond and subfemtosecond x-ray pulses from SASE based free electron laser*, *Phys. Rev. Lett.* **92** (2004) 074801.

[2] E.L. Saldin, E.A. Schneidmiller and M.V. Yurkov, *Statistical properties of the radiation from SASE FEL operating in the linear regime*, *Nucl. Instrum. Meth.* **A 407** (1998) 291.

[3] M. Yabashi, J.B. Hastings, M.S. Zolotorev, H. Mimura, H. Yumoto, S. Matsuyama et al., *Single-shot spectrometry for x-ray free-electron lasers*, *Phys. Rev. Lett.* **97** (2006) 084802.

[4] Y. Inubushi, K. Tono, T. Togashi, T. Sato, T. Hatsui, T. Kameshima et al., *Determination of the pulse duration of an X-ray free electron laser using highly resolved single-shot spectra*, *Phys. Rev. Lett.* **109** (2012) 144801.

[5] T. Katayama, Y. Inubushi, Y. Obara, T. Sato, T. Togashi, K. Tono et al., *Femtosecond X-ray absorption spectroscopy with hard X-ray free electron lasers*, *Appl. Phys. Lett.* **103** (2013) 131105.

[6] D. Zhu, M. Cammarata, J.M. Feldkamp, D.M. Fritz, J.B. Hastings, S. Lee et al., *A single-shot transmissive spectrometer for hard X-ray free electron lasers*, *Appl. Phys. Lett.* **101** (2012) 034103.

[7] D. Rich, D. Zhu, J. Turner, D. Zhang, B. Hill and Y. Feng, *The LCLS variable-energy hard X-ray single-shot spectrometer*, *J. Synchrotron Rad.* **23** (2016) 3.

[8] J. Amann, W. Berg, V. Blank, F.-J. Decker, Y. Ding et al., *Demonstration of self-seeding in a hard-X-ray free-electron laser*, *Nat. Photonics* **6** (2012) 693.

[9] U. Boesenberg, L. Samoylova, T. Roth, D. Zhu, S. Terentyev, M. Vannoni, Y. FENG, T. Brandt van Driel, S. Song, V. Blank, H. Sinn, A. Robert, A. Madsen, X-ray spectrometer based on a bent diamond crystal for high repetition rate free-electron laser applications, *Opt. Express* **25** (2017) 2852.

[10] P. Karvinen, S. Rutishauser, A. Mozzanica, D. Greiffenberg, P.N. Juranić, A. Menzel et al., *Single-shot analysis of hard X-ray laser radiation using a noninvasive grating spectrometer*, *Opt. Lett.* **24** (2012) 5073.

[11] T. Katayama, S. Owada, T. Togashi, K. Ogawa, P. Karvinen, I. Vartiainen et al., *A beam branching method for timing and spectral characterization of hard X-ray free-electron lasers*, *Struct. Dynam.* **3** (2016) 034301.

[12] J. Rehanek, F. Schäfers, A. Erko, M. Scheer, W. Freund, J. Grünert et al., *Simulations of diagnostic spectrometers for the European XFEL using the ray-trace tool RAY*, *Proc. SPIE* **8141** (2011) 814109.

[13] J. Rehanek, F. Schäfers, H. Löchel, A. Firsov, J. Grünert, W. Freund et al., *A case study of novel X-ray Optics for FEL sources*, *J. Phys. Conf. Ser.* **425** (2013) 052013.

2017 JINST 12 P05024

[14] H. Löchel, M. Brzhezinskaya, A.Firsov, J. Rehanek and A. Erko, *Reflection zone plates for 2D focusing and spectroscopy of hard X-rays*, *J. Phys. Conf. Ser.* **425** (2013) 052025.

[15] H. Löchel, C. Braig, M. Brzhezinskaya, F. Siewert, P. Baumgärtel, A. Firsov et al., *Femtosecond high-resolution hard X-ray spectroscopy using reflection zone plates*, *Opt. Express* **23** (2015) 8788.

[16] C. Braig, H. Löchel, A. Firsov, M. Brzhezinskaya, A. Hafner, J. Rehanek et al., *Hard X-ray spectroscopy and imaging by a reflection zone plate in the presence of astigmatism*, *Opt. Lett.* **41** (2016) 29.

[17] M. Makita, P. Karvinen, V.A. Guzenko, N. Kujala, P. Vagovic and C. David, *Fabrication of diamond diffraction gratings for experiments with intense hard X-rays*, *Microelectron. Eng.* **176** (2017) 75.

[18] M. Makita, P. Karvinen, D. Zhu, P.N. Juranic, J. Grünert, S. Cartier et al., *High-resolution single-shot spectral monitoring of hard X-ray free-electron laser radiation*, *Optica* **2** (2015) 912.

[19] T. Kroll, J. Kern, M. Kubin, D. Ratner, S. Gul, F.D. Fuller et al., *X-ray absorption spectroscopy using a self-seeded soft X-ray Free-Electron Laser*, *Opt. Express* **24** (2016) 22469.

[20] C. David, B. Nöhammer, H.H. Solak and E. Ziegler, *Differential X-ray phase contrast imaging using a shearing interferometer*, *Appl. Phys. Lett.* **81** (2002) 3287.

[21] D. Zhu, M. Cammarata, J. Feldkamp, D.M. Fritz, J. Hastings, S. Lee et al., *Design and operation of a hard x-ray transmissive single-shot spectrometer at LCLS*, *J. Phys. Conf. Ser.* **425** (2013) 052033.

[22] M. Makita, P. Karvinen, V.A. Guzenko, N. Kujala, P. Vagovic and C. David, *Fabrication of diamond diffraction gratings for experiments with intense hard X-rays*, *Microelectron. Eng.* **176** (2017) 75.

[23] M. Born and E. Wolf, *Principles of Optics — Electromagnetic Theory of Propagation, Interference and Diffraction of Light*, 6$^{\text{th}}$ edition, Pergamon Press (1980), pp. 540–541.

[24] U. Flechsig, A. Jaggi, S. Spielmann, H.A. Padmore and A.A. MacDowell, *The optics beamline at the Swiss Light Source*, *Nucl. Instrum. Meth.* **A 609** (2009) 281.

[25] J.C.M. Brentano, *An X-ray goniometer using beams of large aperture for photographically recording crystal-powder reflections*, *P. Phys. Soc.* **49** (1937) 61.

2017 JINST 12 P05024